Supplementary Information (SI) for Energy & Environmental Science.
This journal is © The Royal Society of Chemistry 2025

Supporting Information

Scalable Copper Current Collectors with Precisely Engineered Lithiophilic Alloy "Skins" for Durable Lithium-Metal Batteries

Huiqun Wang,[a,§] Yuxiang Mao,[a,§] Peng Xu,[a] Yu Ding,[a] Huiping Yang,[a] Jian-Feng Li,[a] Yu Gu,*[a] Jiajia Han,*[b] Li Zhang,*[a] Bing-Wei Mao[a]

[a]College of Chemistry and Chemical Engineering, State Key Laboratory of Physical Chemistry of Solid Surfaces, The MOE Key Laboratory of Spectrochemical Analysis and Instrumentation, Tan Kah Kee Innovation Laboratory, Collaborative Innovation Center of Chemistry for Energy Materials (iChEM), Xiamen University, Xiamen 361005, Fujian, China. E-mail: ygu@xmu.edu.cn; zhangli81@xmu.edu.cn

[b]College of Materials, Fujian Key Laboratory of Surface and Interface Engineering for High Performance Materials, Xiamen Key Laboratory of High Performance Metals and Materials, Xiamen University, Xiamen, 361005, Fujian, China. Email: jiajiahan@xmu.edu.cn

H. Wang and Y. Mao contributed equally to this work.

Experimental Methods

Materials

Cu foils (9 μm), Zn foils (0.2 mm) and $LiFePO_4$ (LFP) were purchased from Shenzhen Kejing Technology Co., Ltd. Li foils (12 mm, 1 mm) were obtained from China Energy Lithium Co., Ltd. $LiNi_{0.9}Co_{0.05}Mn_{0.05}O_2$ (NCM90), glass fiber membranes (GF/D, Whatman) for ISOM, baseline commercial electrolytes of 1 M $LiPF_6$/EC-DMC-DEC (1:1:1, v/v) with 10% FEC and 2% VC and 1 M LiTFSI/DOL-DME (1:1, v/v) with 2 wt% $LiNO_3$ were sourced from Dongguan Keludi New Energy Technology Co., Ltd. The cathodes were prepared by mixing the active substance, Super-P, and poly(vinylidene difluoride) at a mass ratio of 90:5:5 in N-methyl 2-pyrrolidone to form a slurry. This slurry was then coated onto a carbon-coated Al foil, cut into discs with a diameter of 11 mm. and dried overnight at 100 °C in a vacuum oven. In coin cells, the average mass loadings of regular NCM90 and LFP cathodes were approximately 3.5 mg cm^{-2} and 5.5 mg cm^{-2}, respectively, while the high-loading LFP had a mass loading of about 18 mg cm^{-2}. In pouch cells, the mass loadings of NCM90 and LFP cathodes were approximately 15.8 mg cm^{-2} and 13.8 mg cm^{-2}, respectively.

Preparation of copper current collectors with alloyed skins

Commercial Cu foil was firstly punched into discs (19 mm, 9 μm) and rinsed using a sequence of diluted hydrochloric acid, acetone, deionized water and ethanol to remove any impurities. Zinc foil was similarly punched into circular pieces (19 mm, 0.2 mm) and scrubbed with wet wipes. The Cu with the Zn disks were aligned and placed on a conveyor belt before screwed to the cathode and anode electrodes of the Joule heating device in an argon-filled glovebox (Mikrouna), with O_2 and H_2O contents below 0.1 ppm. The Joule heating device was powered on approximately 30 W and stabilized for 120 s to produce a current collector (CC) with the surface primarily composed mainly of Cu_5Zn_8 (denoted as Cu@Cu_5Zn_8). This CC was then moved to the next position by the conveyor belt to receive a higher power pulse, resulting in the transformation of Cu@Cu_5Zn_8 into Cu@$Cu_{0.64}Zn_{0.36}$. The power applied during the two-step Joule heating process, along with the duration and distance between materials, need to be strictly controlled.

Materials characterization

The structures of Cu-Zn alloys were analyzed using XRD profiles recorded with a Rigaku Ultima IV diffractometer, employing Cu Kα radiation (λ = 1.54056 Å) at 40 kV and 30 mA. The morphologies of Cu-Zn alloys and the plated Li metal on various CCs were characterized by FESEM (Gemini SEM 500), AFM (SPM 5500), and TEM (JEOL JEM-2100plus). Prior to analysis, samples were rinsed with dimethyl carbonate (DMC) solvent to remove residual electrolytes and then dried in the vacuum chamber of the argon-filled glove box. For TEM sample preparation, a micro-grid membrane was directly placed on the Joule heating device, where Cu nanoparticles were first deposited, followed by alloying. AFM measurements were conducted within an argon-filled glove box. Wetting tests of molten Li on different CC surfaces were carried out at temperature over 200 °C on a stainless pan in an argon-filled glove box. XPS measurements were performed on Thermo Scientific ESCALAB Xi+ using monochromatic Al Kα radiation (1486.6 eV) at 24 W and 16 KV. The in situ optical microscopy experiment of Li deposition involved wrapping Li around a 200 µm Cu foil to serve as the counter electrode, placing it in a 1.7 mL, 5 mm path length cuvette. The two electrodes were separated by a GFD membrane, and Li deposition was observed in situ under a metallographic microscope at a current density of 5 mA cm^{-2}. The contents of Cu, Zn, Sn, Ag, Al, Mg were quantified using inductively ICP-OES (SPECTROBLUEFMX36).

Electrochemical measurements

Electrochemical tests were conducted utilizing CR2032-tyoe coin cells, assembled in an argon-filled glovebox (O_2 < 0.1 ppm, H_2O < 0.1 ppm). For electrochemical testing, 80 µL of electrolyte was added to each coin cell, while in pouch cells, 0.8 mL of electrolyte was used with Li metal anodes having a fixed areal capacity of 4 mAh cm^{-2}. The resistances of SEI (R_{SEI}) and charge transfer resistance (R_{ct}) were determined from EIS on a Metrohm Autolab electrochemical workstation in the frequency range of 10^{-2} ~10^{5} Hz with a 5 mV amplitude AC signal. Cyclic voltammetry measurements were conducted at a constant scan rate of 0.1 mV s^{-1} with a potential window between -0.05 to 2 V (vs. Li^{+}/Li), using a CHI660E electrochemical workstation (Chenhua Instruments). Li||Cu cells were constructed with Li metal as the

counter electrode and Cu foil as the working electrode, using a Celgard-2325 separator soaked in either 1 M $LiPF_6$/EC-DMC-DEC (1:1:1, v/v) with 10% FEC and 2% VC or 1 M LiTFSI/DOL-DME (1:1, v/v) with 2 wt% $LiNO_3$ electrolytes. Each cell needs to be activated for 5 cycles in a potential range of 0–1 V under 0.1 mA cm^{-2}, followed by the deposition of 1.0 mAh cm^{-2} of Li on the substrate at the current density of 1.0 mA cm^{-2}.

Galvanostatic intermittent titration technique (GITT) test involved depositing Li on the CCs at a current density of 0.5 mA cm^{-2} for 8 h to form a metallic Li layer approximately 20 μm thick. Subsequently, Li was intermittently deposited 120 times at 1 mA cm^{-2} for 30 s per cycle, with a 2-min rest period between cycles. The stripping process followed a similar protocol.[1] The Li||Li symmetrical cells were based on the Li||Cu cells, with a charge of 4.0 mAh cm^{-2} of Li was pre-deposited on the various Cu CCs, followed by symmetric cycling at 1.0 mAh cm^{-2}. Tafel plots were measured at a scan rate of 0.1 mV s^{-1} in symmetrical Li cells, with a potential range of -0.2 to 0.2 V (vs. Li^+/Li). Galvanostatic charge/discharge was performed at various currents from 20 to 120 μA to extract the overpotential and calculate the exchange current density (i^0) using the following equation[2]: $I = \frac{i_0 F \eta}{2RT}$, where η is the total overpotential, F is Faraday's constant, and R is the standard gas constant. The activation energy value was calculated using the Arrhenius equation: $k_{R_{SEI}} = Aexp\,(\frac{-Ea}{RT})$, where E_a is the activation energy, R is the gas constant, T is the test temperature and A is the pre-exponential factor. For the modified Aurbach Coulombic efficiency (CE) measurement of Li metal, accurate CE tests were carried out on Li||Cu cells as proposed by Zhang *et al*.[3] Prior to CE testing, all cells underwent conditioning cycles with 4 mAh cm^{-2} of Li deposited onto the Cu CCs at 1 mA cm^{-2}, followed by complete stripping to 0.5 V. During testing, a Li reservoir (Q_T) of 4 mAh cm^{-2} was initially plated onto Cu CCs, followed by n (n = 19) cycles of Li plating and striping at 1 mAh cm^{-2} (Q_C) and 1 mA cm^{-2}. Subsequently, all Li on the Cu CCs was stripped to 1 V, and the final stripping charge (Q_S), representing the amount of Li remaining after cycling, was measured. The average CE over n cycles was calculated as follows: CE= $\frac{nQ_C + Q_s}{nQ_C + Q_T}$

To further explore the practical application of the ultrathin Li anode, pre-deposited Li anodes were paired with NCM90 or LFP cathodes to form full-cells. Taking the Li||NCM90 full cell as an example, Li||Cu cells were first assembled and subjected to charge-discharge activation for 10 cycles. These cells were then disassembled and paired with NCM90, with 80 µl of 1 M $LiPF_6$/EC-DMC-DEC (1:1:1, v/v) containing 10% FEC and 2% VC added for cycling tests in the voltage range of 3-4.3 V. The Li||LFP full cell followed a similar process, except the electrolyte employed was either 1 M $LiPF_6$/EC-DMC-DEC (1:1:1, v/v) with 10% FEC and 2% VC or 1 M LiTFSI/DOL-DME (1:1 vol%) with 2 wt% $LiNO_3$, and tests were conducted in a voltage range of 2.4-3.8 V.

Calculations

All calculations were conducted by using density functional theory (DFT) as implemented in the Vienna *Ab initio* Simulation Package (VASP)[4-6], with the projector-augmented wave method (PAW)[7] escribing the ion-electron interaction. The valence electrons were taken into account using a plane wave basis set with a kinetic energy cut-off of 600 eV, which guarantees that the total energy was converged to 1 meV per atom. The generalized gradient approximation (GGA) with Perdew–Burke–Ernzerhof (PBE)[8-9] functionals was used to express the interacting electron exchange-correlation energy, with an electronic convergence criterion of 10^{-6} eV and an ionic convergence criterion of 10^{-2} eV $Å^{-1}$. The van der Waals interaction was considered by the empirical correction of Grimme's scheme (DFT-D3)[9]. The supercell of Cu and Cu-Zn alloys with a vacuum gap of 15 Å was taken as the substrate model. The reciprocal space was sampled by a gamma-centered k-mesh with a resolution of 0.03 in the units of 2π/Å, depending on the model. The Von Mises local shear strain was calculated to characterize the deformation degree of the Li layer on the substrate with reference to the Li crystal. Ab initio molecular dynamics (AIMD) simulations are performed in a typical ensemble (NVT), and temperature control is achieved by the Nosé–Hoover thermostat. The motion equations are solved using the velocity Verlet algorithm with a time step of 1 fs (1 fs = 10^{-15} seconds).

The binding energy (E_b) is expressed as:

$$E_b = (E_{total}(n) - E_{total}(n-1) - m * E_{atom})/m$$ Equation S1

where E_{total}(n), E_{total}(n-1), and E_{atom} denote the total energy of substrate with n layers of Li, n-1 layers of Li, and one Li atom, respectively. The value of *m* equals to the number of Li atom per layer.

Supplemental Fig. s and Tables

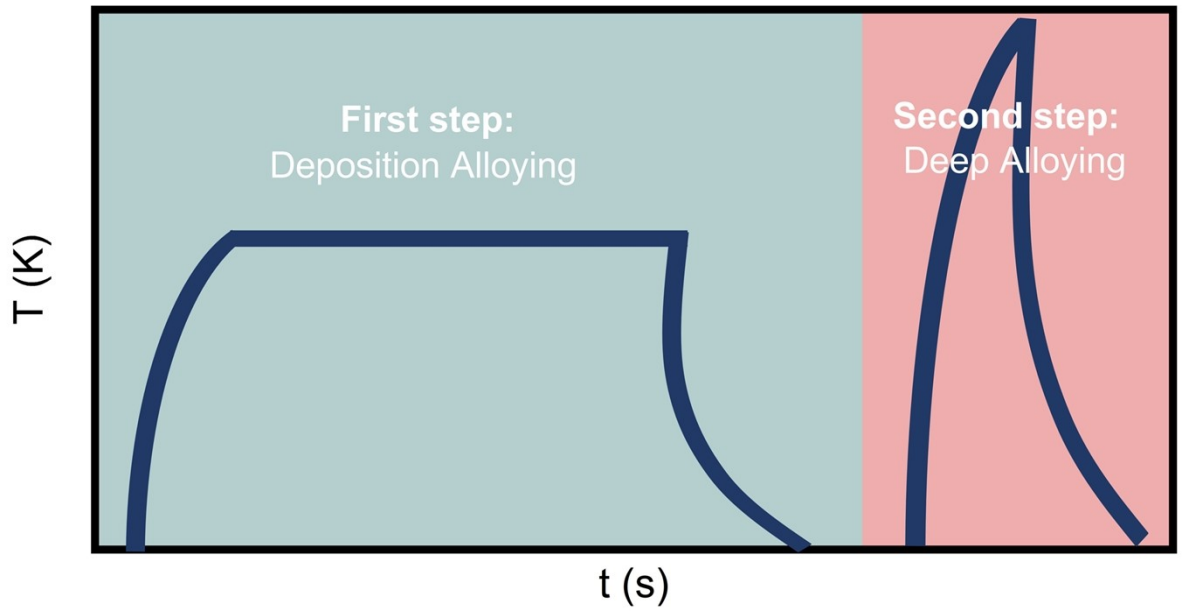

Fig. S1 Simulation of the temperature curve during the UHT preparation process. As shown in the simulated curve, the heating rate of the device is slightly faster than the cooling rate. The operation time in the first step is relatively long, while the second step is ultra-fast.

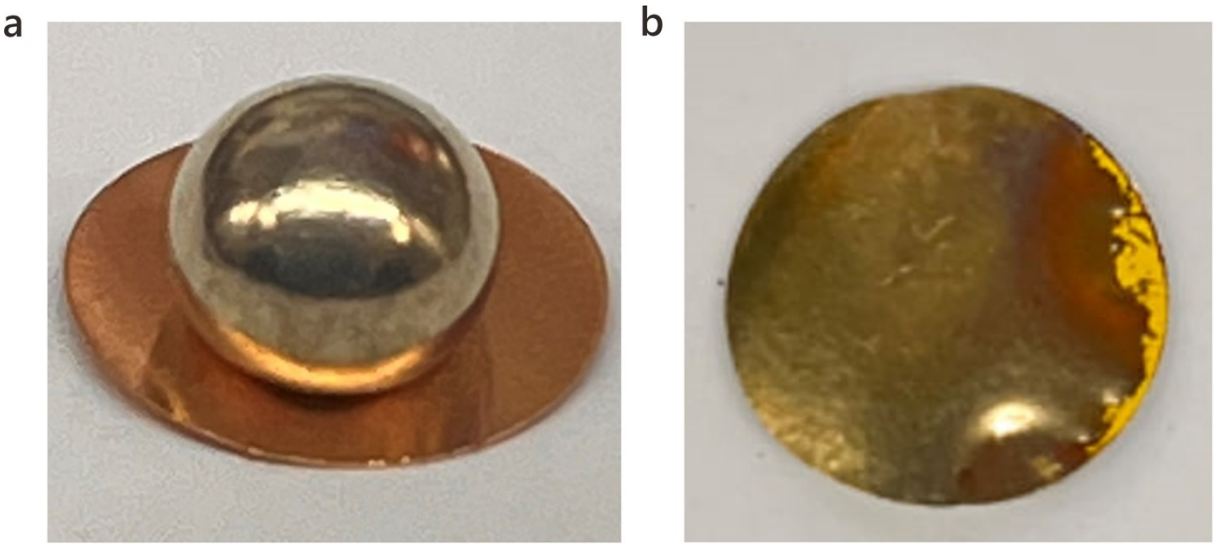

Fig. S2 Digital images of the wettability of molten Li onto (a) Cu and (b) Cu@$Cu_{0.64}Zn_{0.36}$. Due to the presence of the lithiophilic $Cu_{0.64}Zn_{0.36}$ skin modification layer, molten lithium exhibits nearly no wetting on the blank Cu foil, forming a spherical shape, whereas it spreads extensively on the Cu@$Cu_{0.64}Zn_{0.36}$ surface.

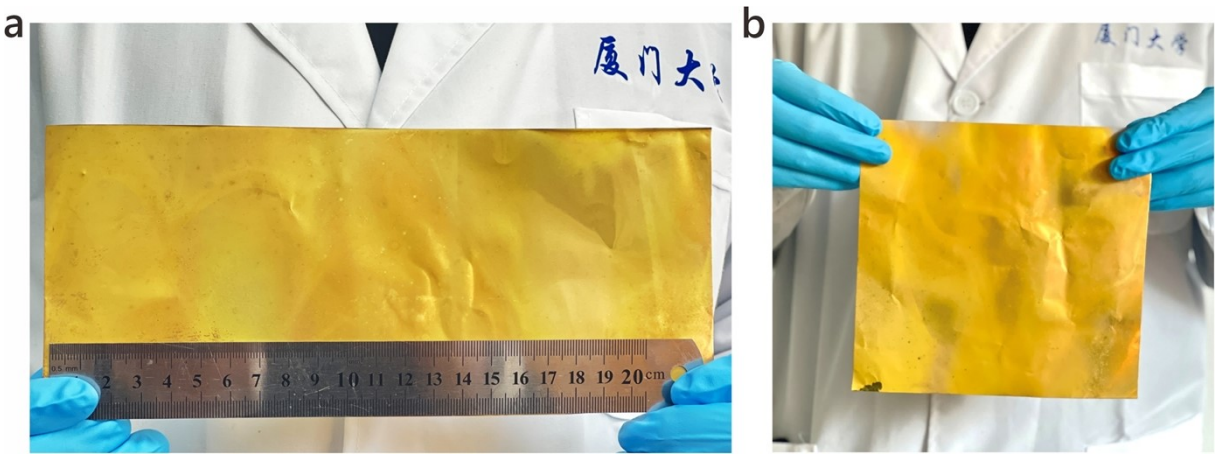

Fig. S3 Digital photographs of the large-sized Cu@$Cu_{0.64}Zn_{0.36}$ samples: (a) 23 cm × 10 cm in length and width, and (b) 19 cm × 18 cm in length and width.

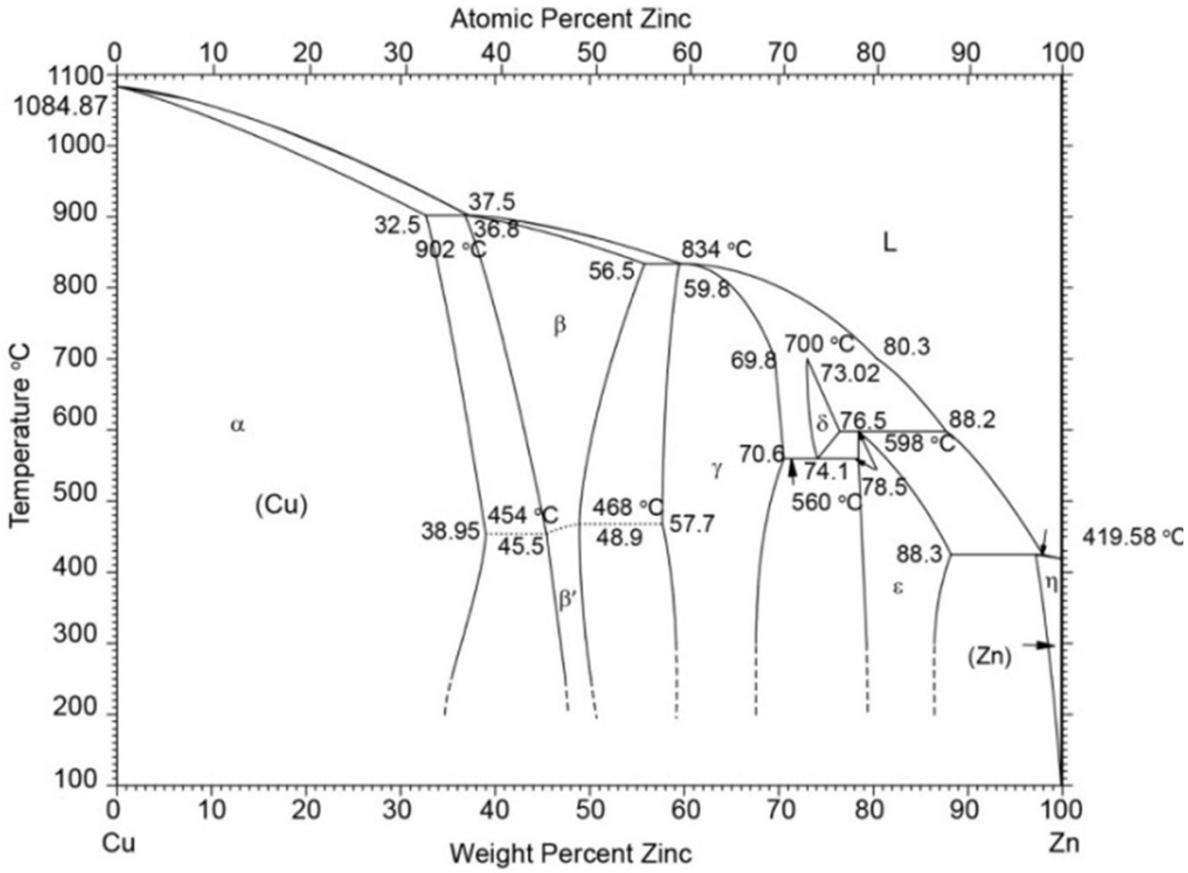

Fig. S4 The binary metal phase diagram of copper and zinc.[10]

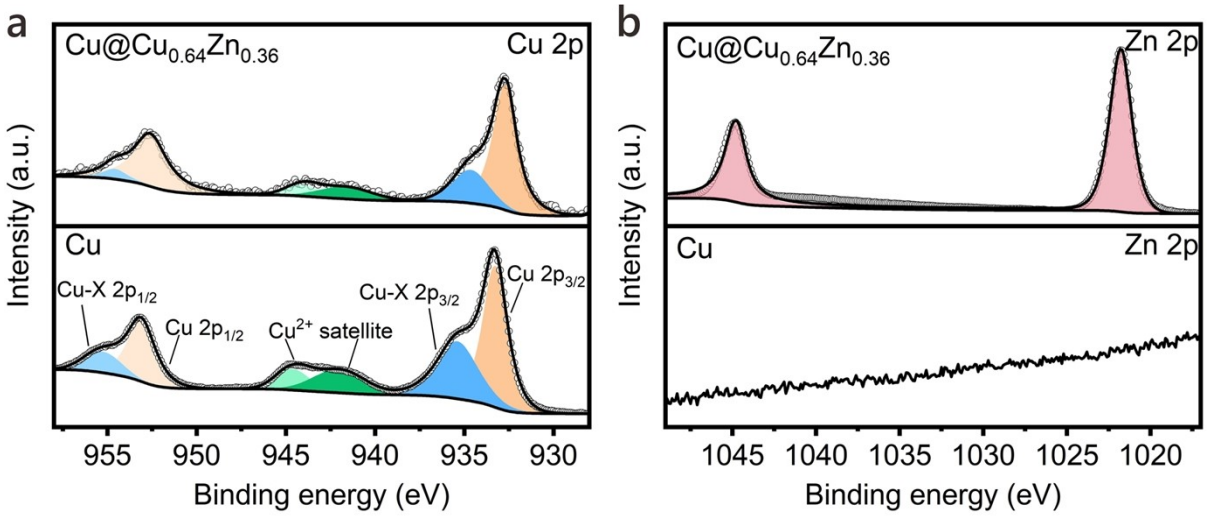

Fig. S5 High-resolution XPS spectra of Cu 2p and Zn 2p of (a) Cu and (b) $Cu@Cu_{0.64}Zn_{0.36}$.

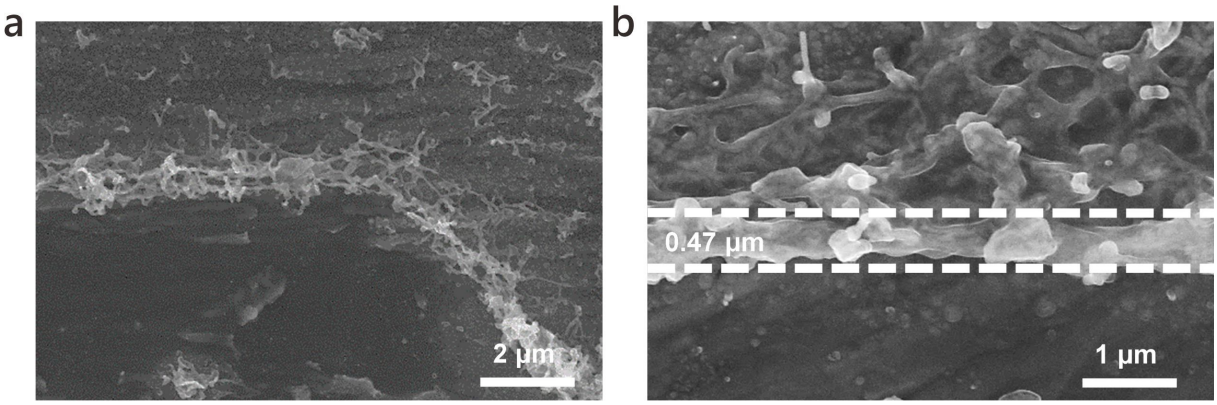

Fig. S6 (a,b) FESEM images of the thickness of $Cu_{0.64}Zn_{0.36}$ layer on Cu foil at different magnifications.

The oily ink isolation method for alloy layers involves applying oily ink to bare Cu foil prior to the UHT treatment. After the UHT processes, the ink was removed using acetone, enabling the observation of the thickness of the $Cu_{0.64}Zn_{0.36}$ alloy layer.

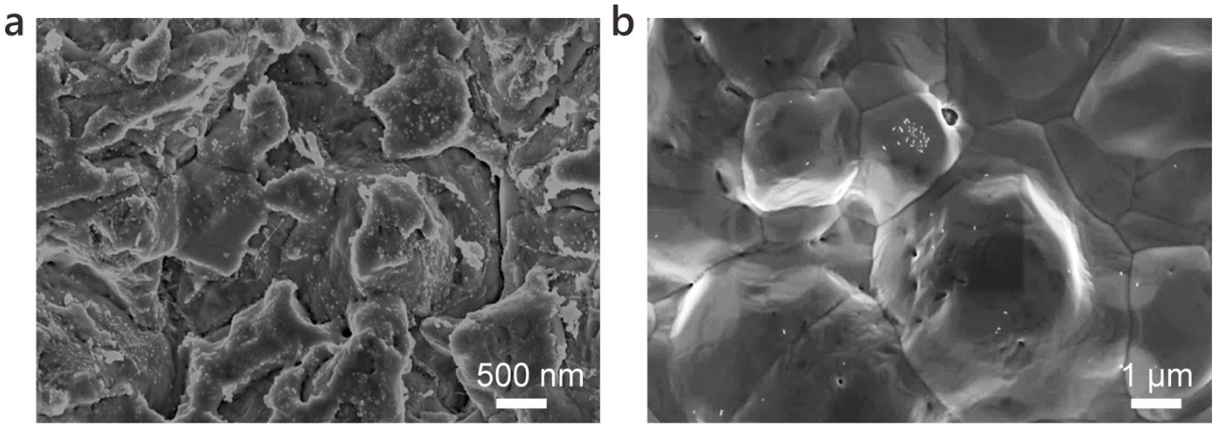

Fig. S7 (a,b) FESEM images of Cu-Zn alloy morphology formed under suboptimal reaction conditions during UHT processes.

Fig. S7a illustrates the effects of an excessively close distance between the Cu foil and Zn foil during Step II. This proximity results in excessive local deposition and clumping after alloying. Fig. S7b demonstrates the consequences of an overly high temperature during Step III, where the Cu foil undergoes simultaneous heating and alloying, leading to extensive melting.

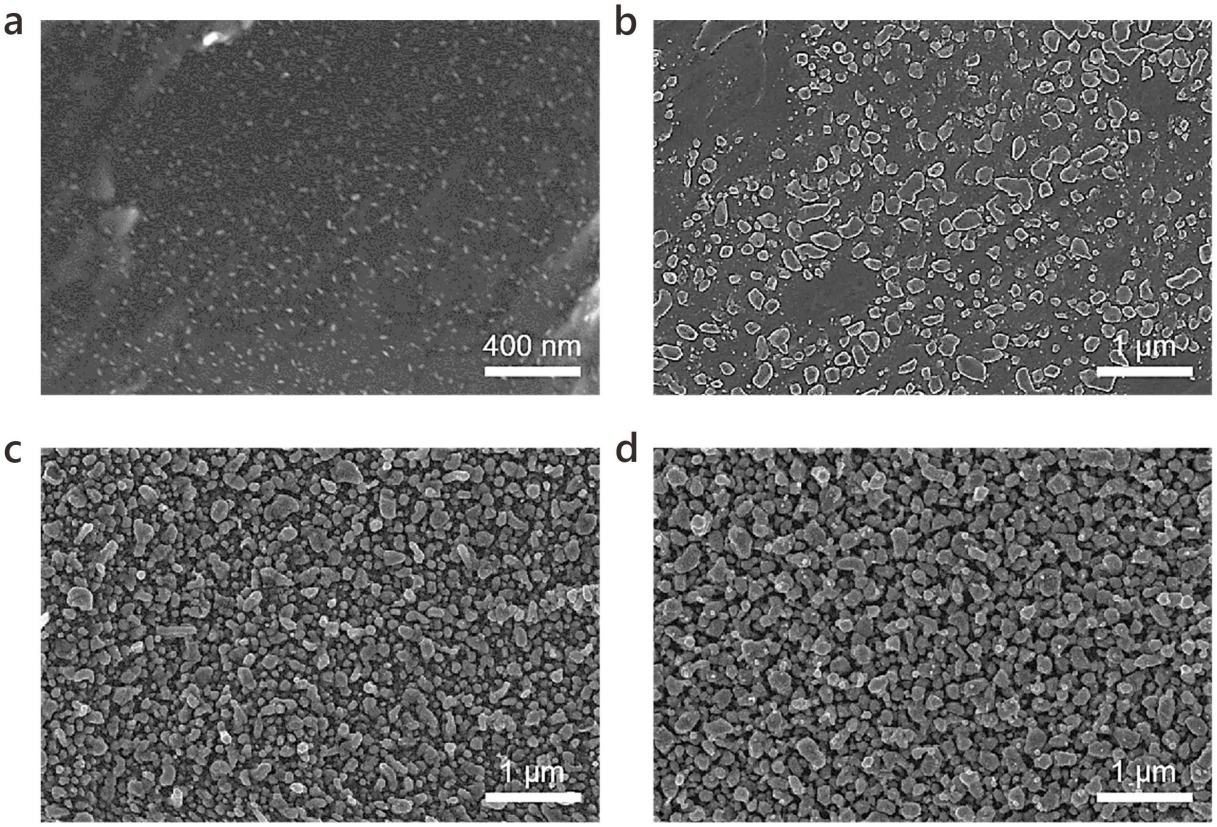

Fig. S8 FESEM images of Cu@Cu_5Zn_8 obtained at different times during the first step of Joule heating on Cu foil: (a) 10 s, (b) 20 s, (c) 120 s and (d) 240 s.

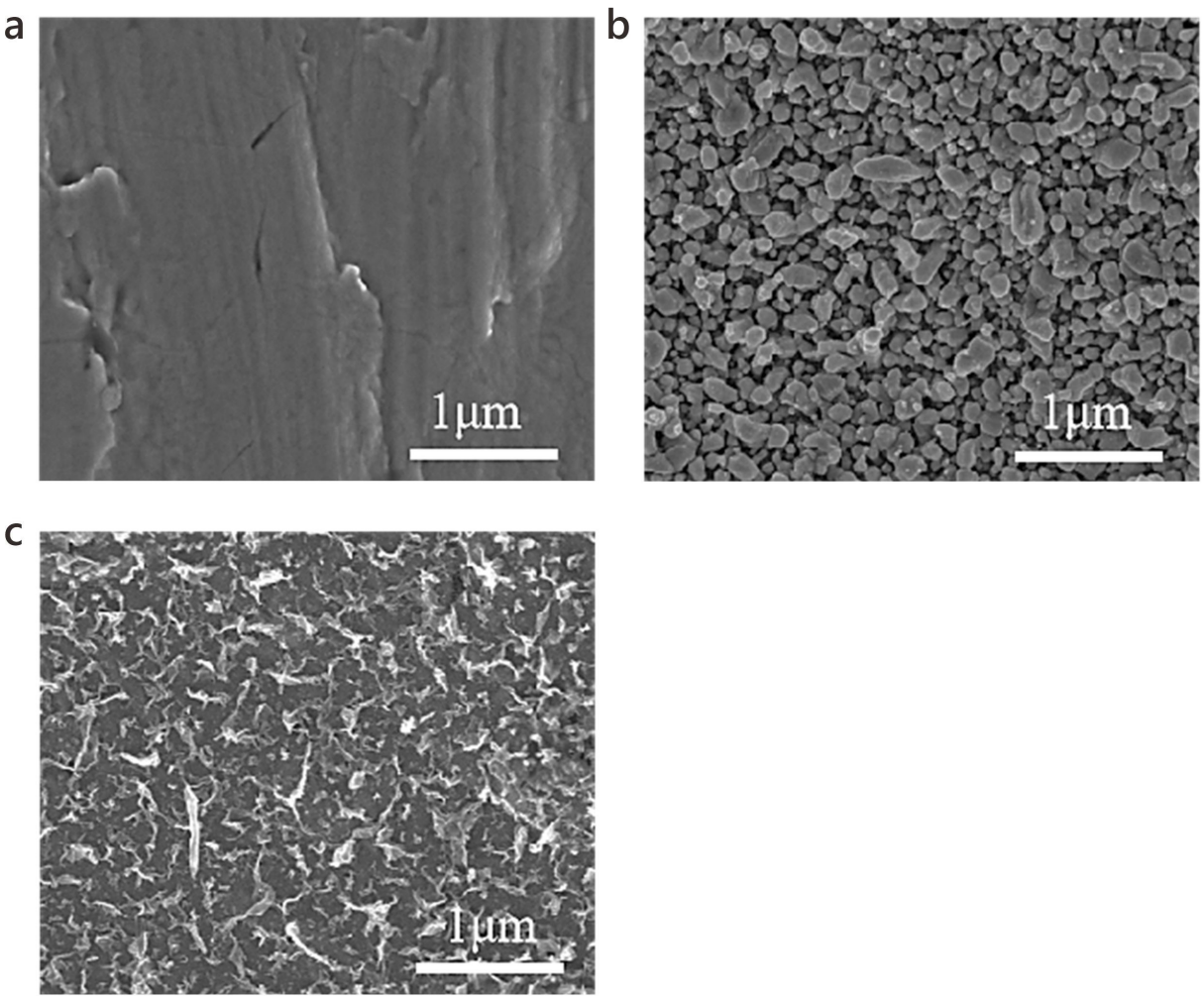

Fig. S9 FESEM images of (a) Cu, (b) Cu@Cu_5Zn_8, and (c) Cu@$Cu_{0.64}Zn_{0.36}$.

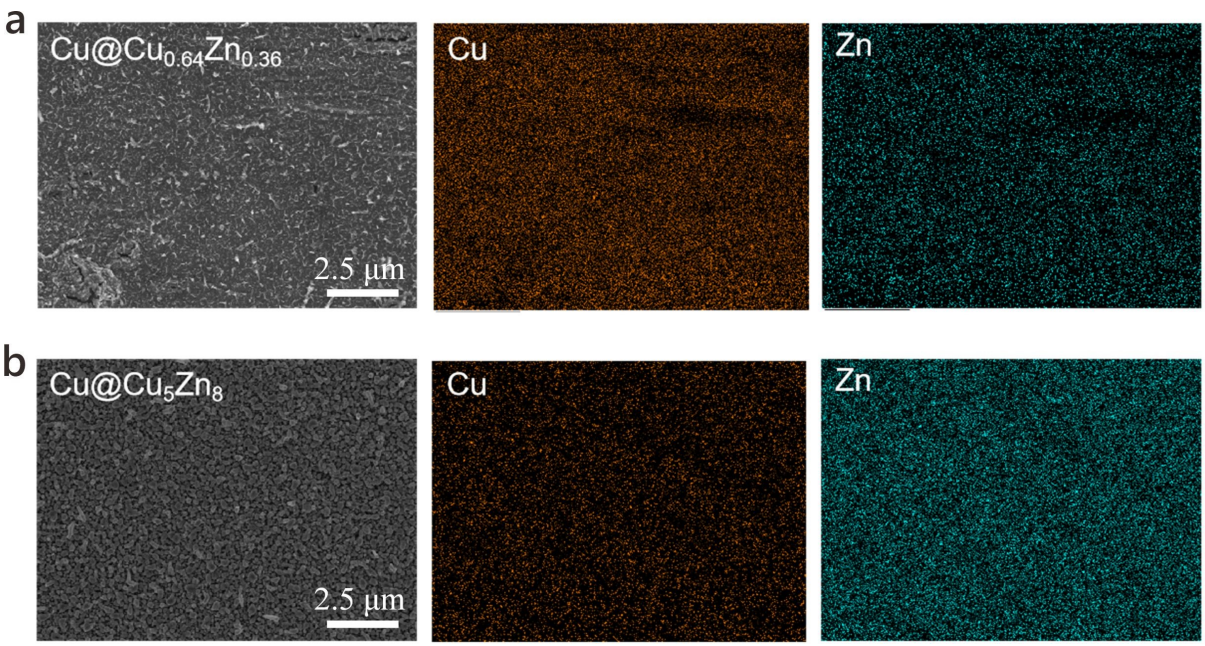

Fig. S10 FESEM images and the corresponding EDX mapping images of (a) $Cu@Cu_{0.64}Zn_{0.36}$ and (b) $Cu@Cu_5Zn_8$.

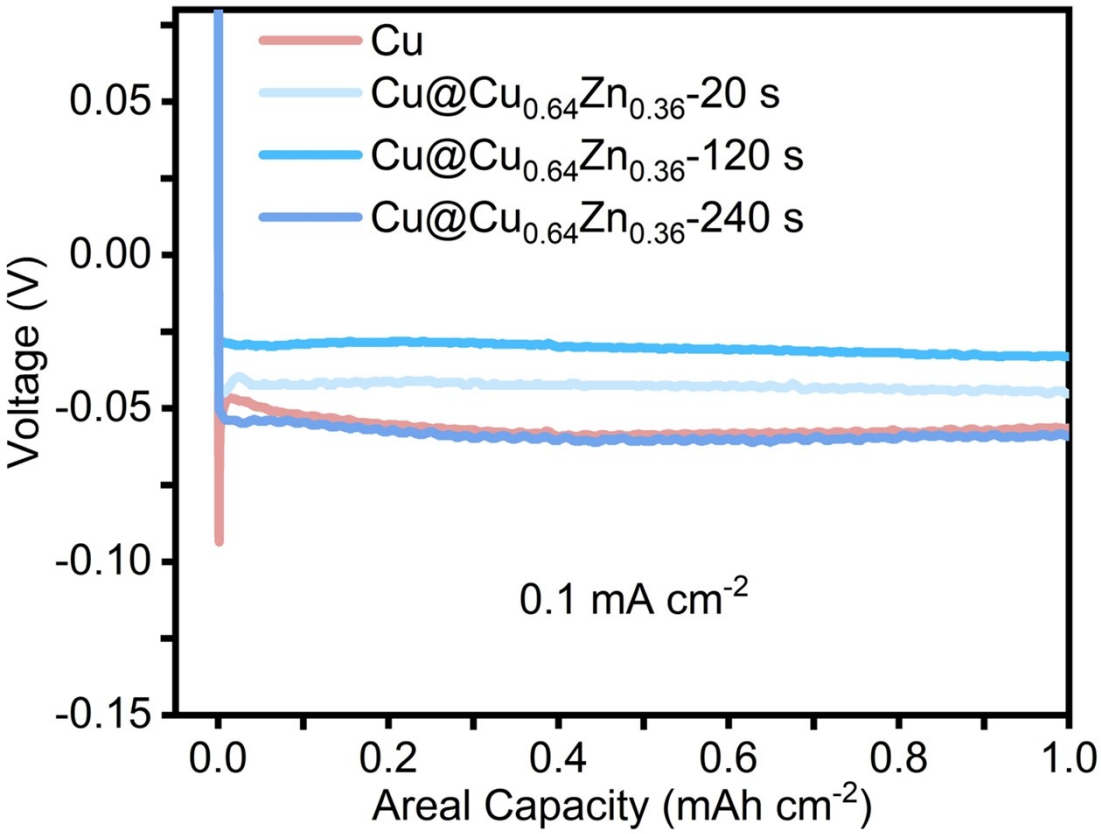

Fig. S11 Voltage-capacity profiles of Li||Cu cells using Cu and Cu@$Cu_{0.64}Zn_{0.36}$ prepared with varying deposition times during stage II of UHT method.

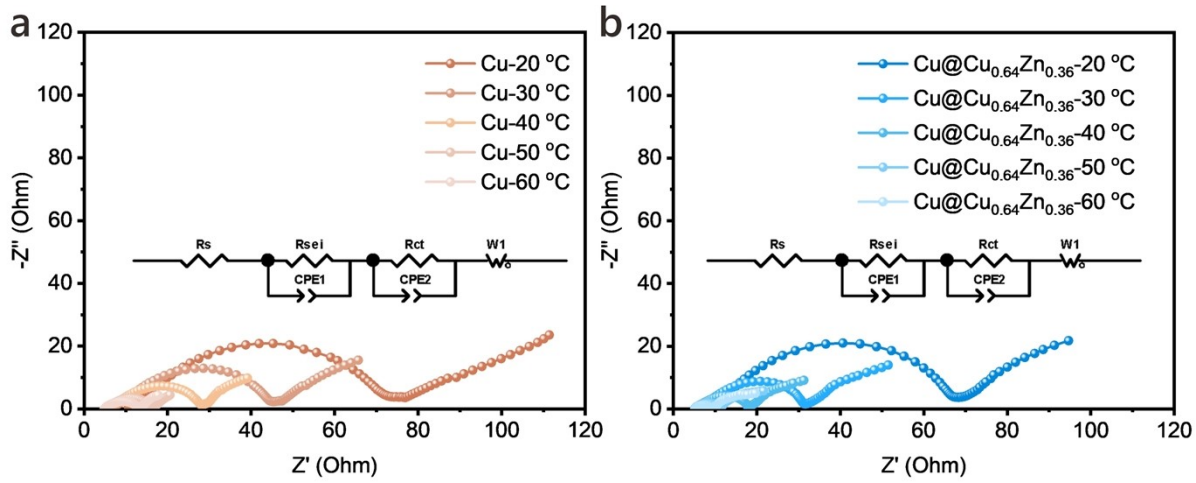

Fig. S12 Nyquist plots for the EIS response of Li||Cu cells with (a) Cu and (b) $Cu@Cu_{0.64}Zn_{0.36}$ at different temperatures, with the equivalent circuit diagrams shown in the insets.

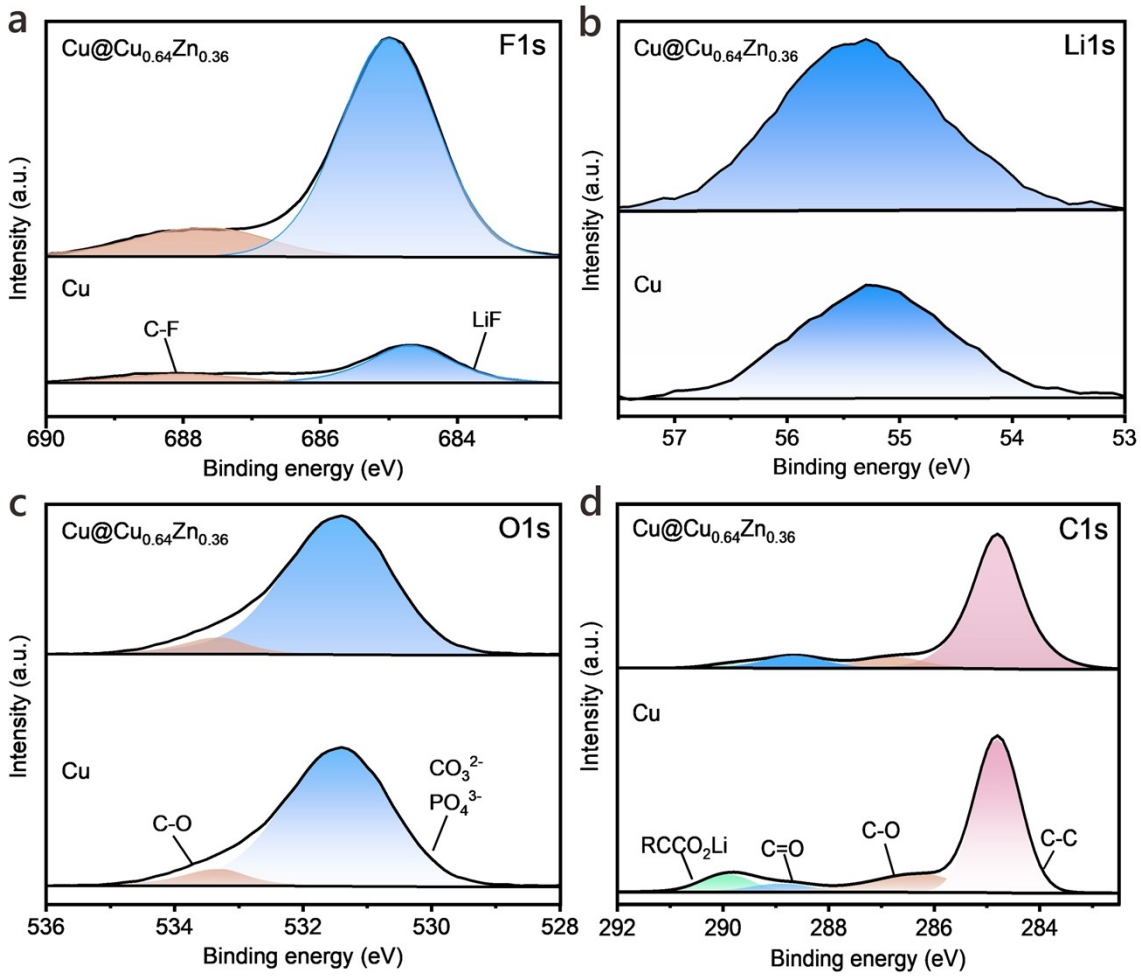

Fig. S13 High-resolution XPS spectra of (a) F 1s, (b) Li 1s, (c) O1s and (d) C 1s of SEIs formed on Cu and $Cu@Cu_{0.64}Zn_{0.36}$.

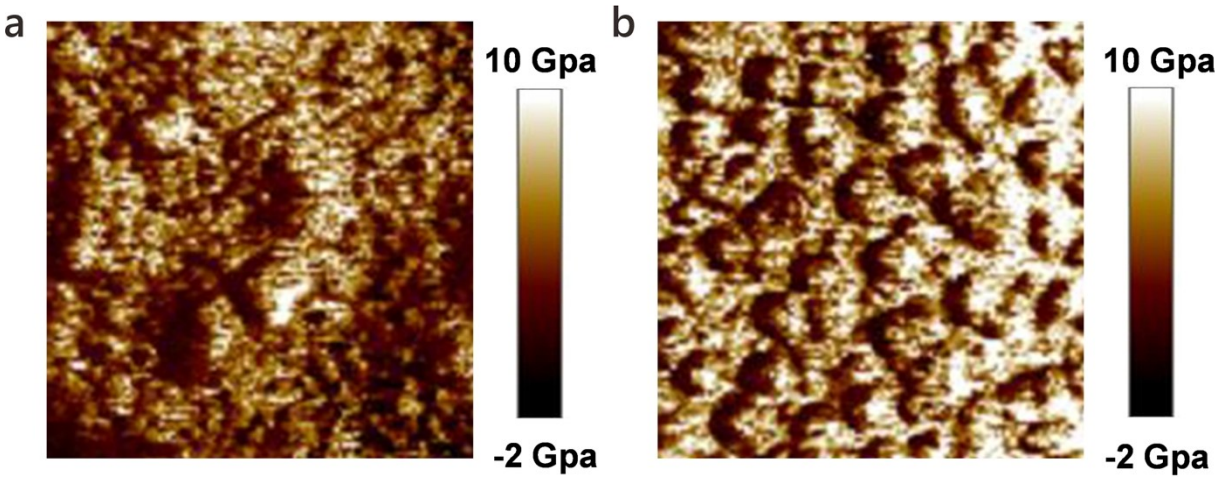

Fig. S14 AFM images showing the mapping of Young's modulus for SEIs on (a) Cu and (b) Cu@$Cu_{0.64}Zn_{0.36}$, respectively, after 5 cycles.

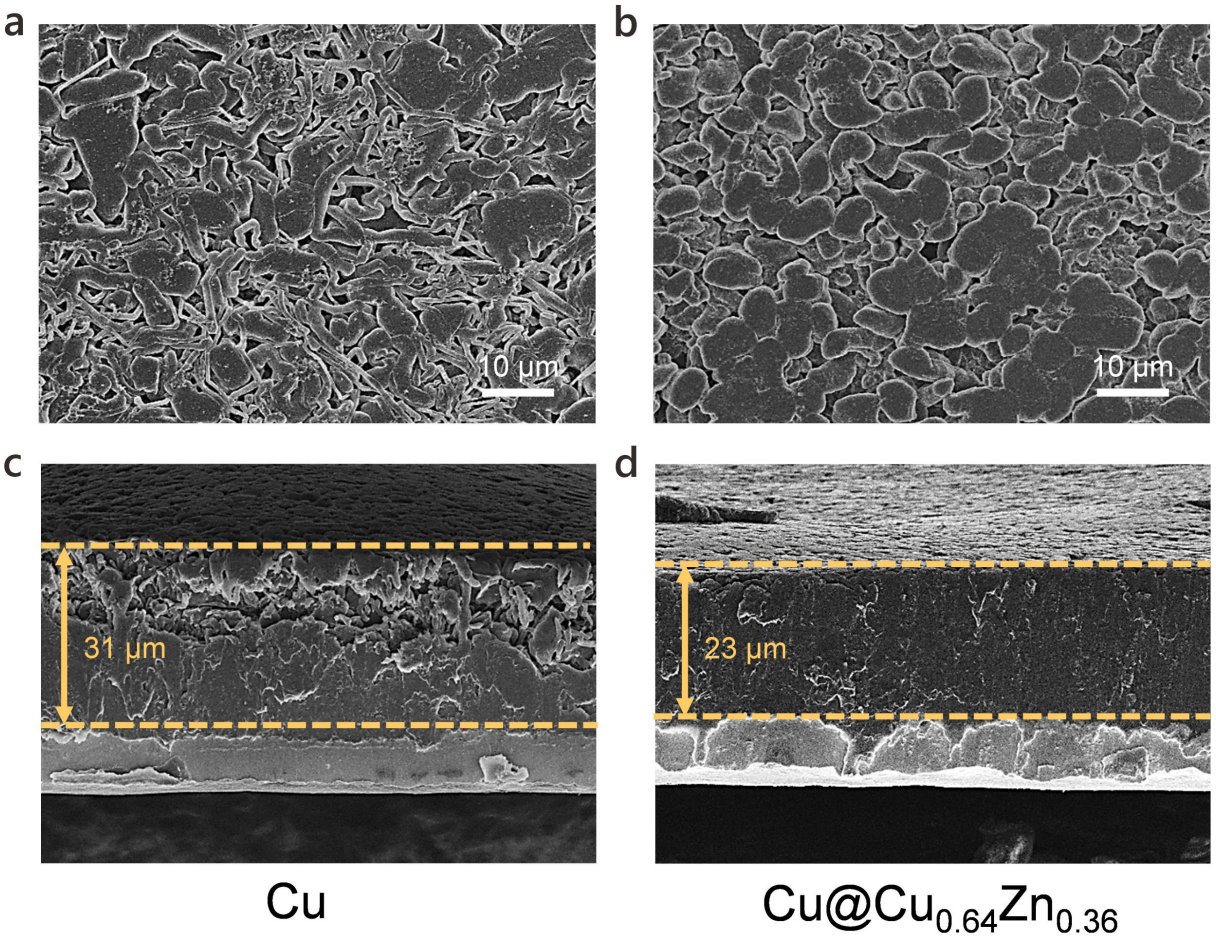

Fig. S15 Top and cross-sectional FESEM images of 4 mAh cm^{-2} of Li deposited on (a, c) Cu and (b, d) $Cu@Cu_{0.64}Zn_{0.36}$ at 1 mA cm^{-2} in Li||Cu cells.

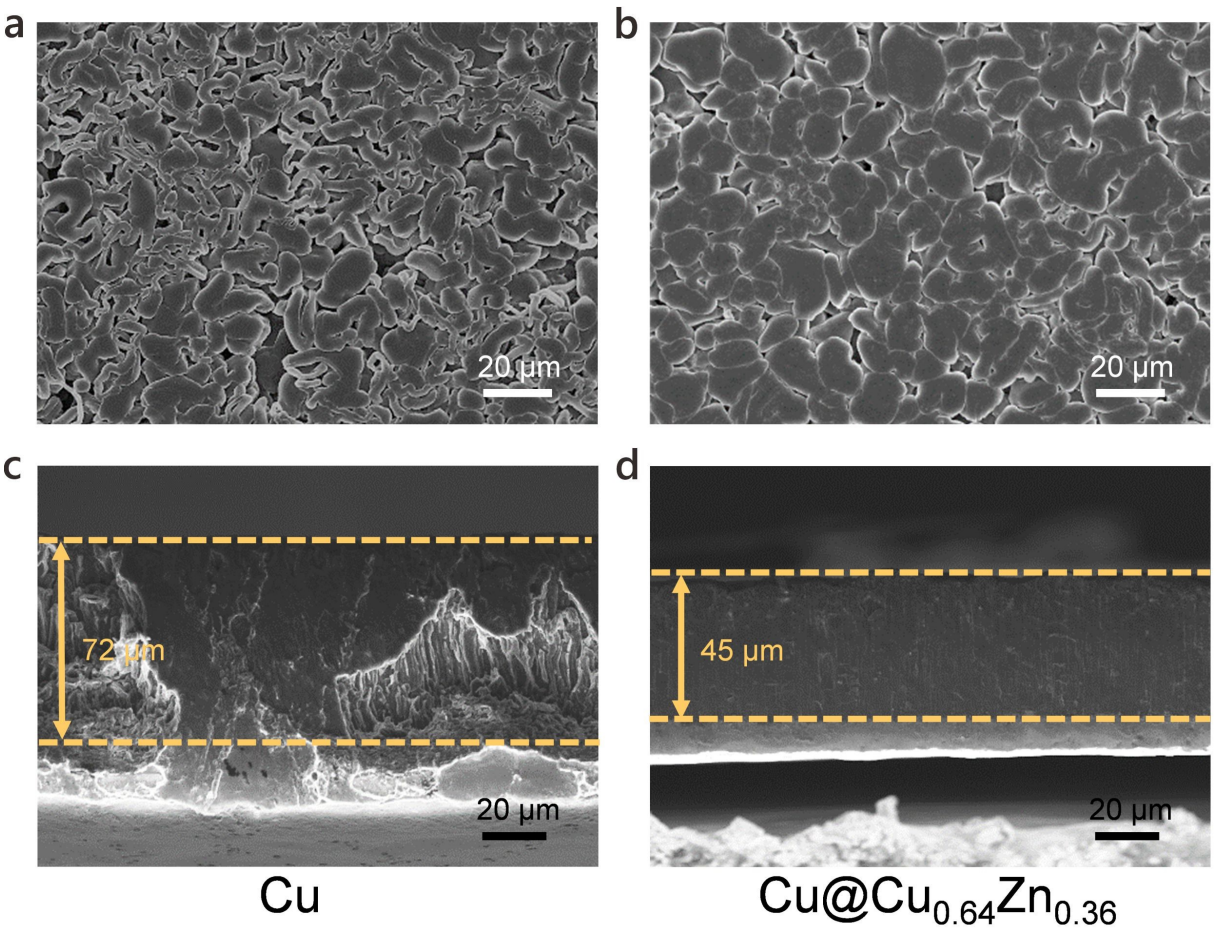

Fig. S16 Top and cross-sectional FESEM images of 10 mAh cm^{-2} of Li deposited on (a, c) Cu and (b, d) $Cu@Cu_{0.64}Zn_{0.36}$ at 1 mA cm^{-2} in Li||Cu cells.

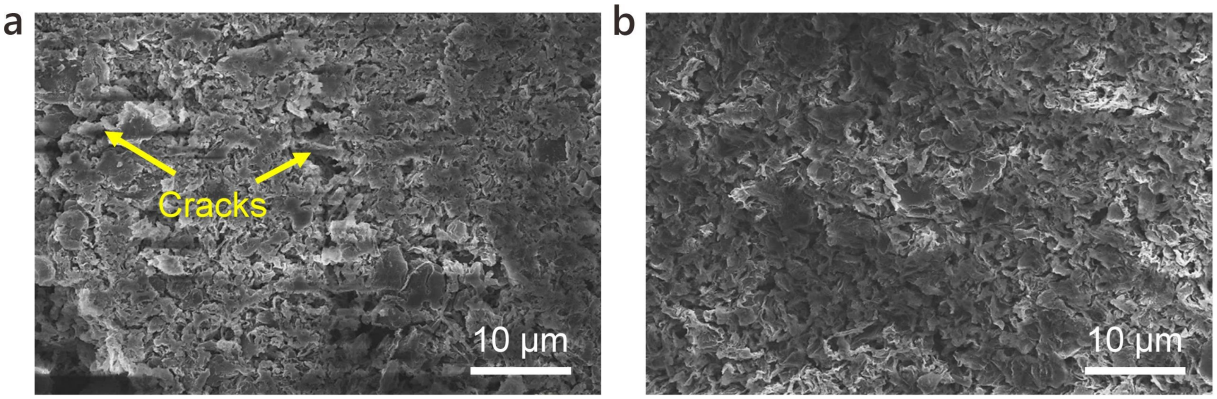

Fig. S17 FESEM images of deposited Li on (a) Cu and (b) Cu@$Cu_{0.64}Zn_{0.36}$ under 1 mA cm^{-2} in Li||Cu cells after 50 cycles.

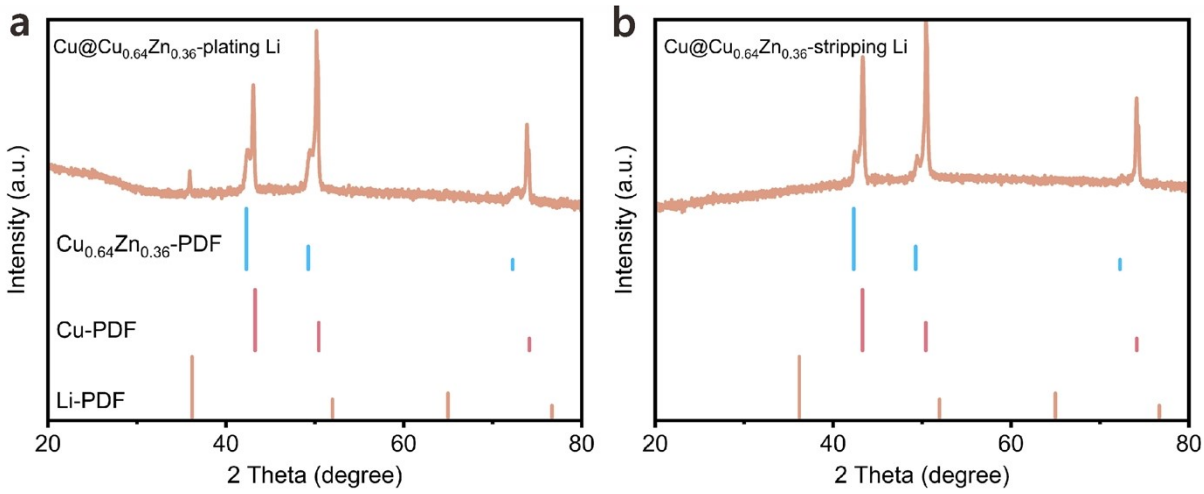

Fig. S18 XRD patterns of $Cu@Cu_{0.64}Zn_{0.36}$ after first Li cycling: (a) plating and (b) stripping Li.

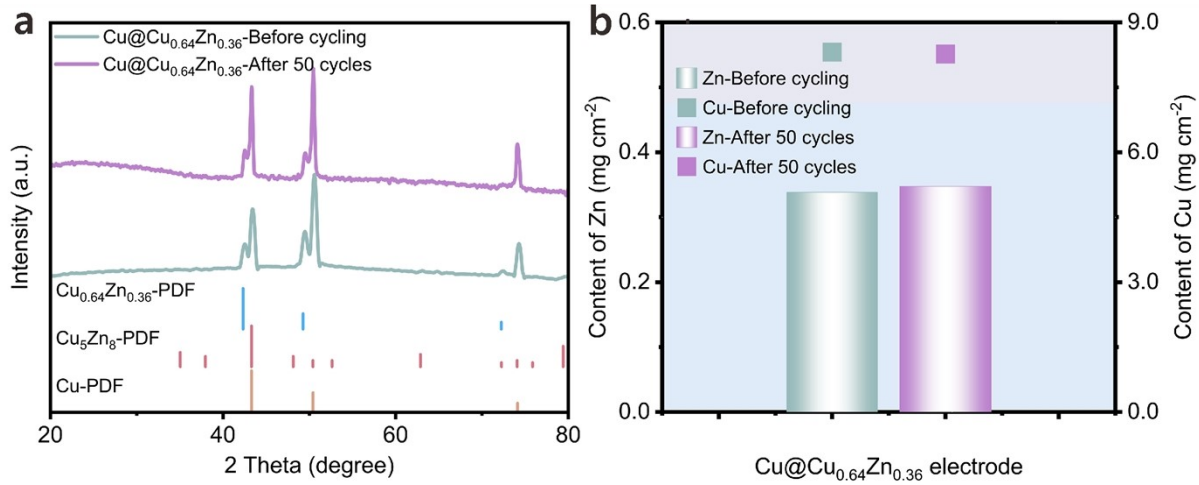

Fig. S19 (a) XRD pattern of $Cu@Cu_{0.64}Zn_{0.36}$ before cycling and after 50 cycles in Li||Cu cell at 1 mA cm^{-2} and 1 mAh cm^{-2}. (b) ICP-OES analysis for Cu and Zn content before cycling and after 50 cycles, with a deposition time of 120 s.

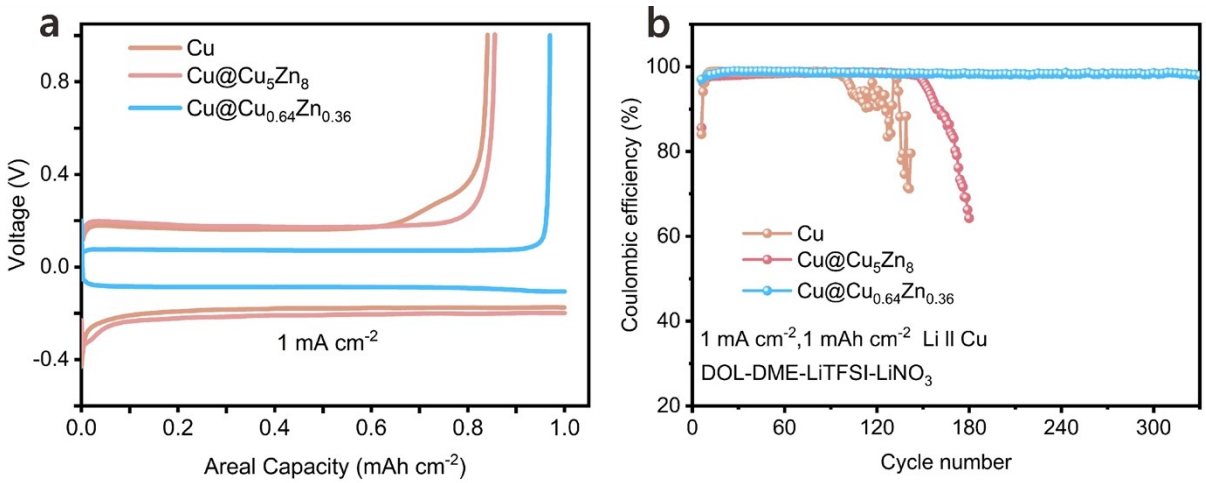

Fig. S20 (a) The initial voltage-capacity curves of Li||Cu cells using Cu, Cu@Cu_5Zn_8, and Cu@$Cu_{0.64}Zn_{0.36}$. (b) Comparison of long-term cycling performance of Li||Cu cells using Cu, Cu@Cu_5Zn_8, and Cu@$Cu_{0.64}Zn_{0.36}$.

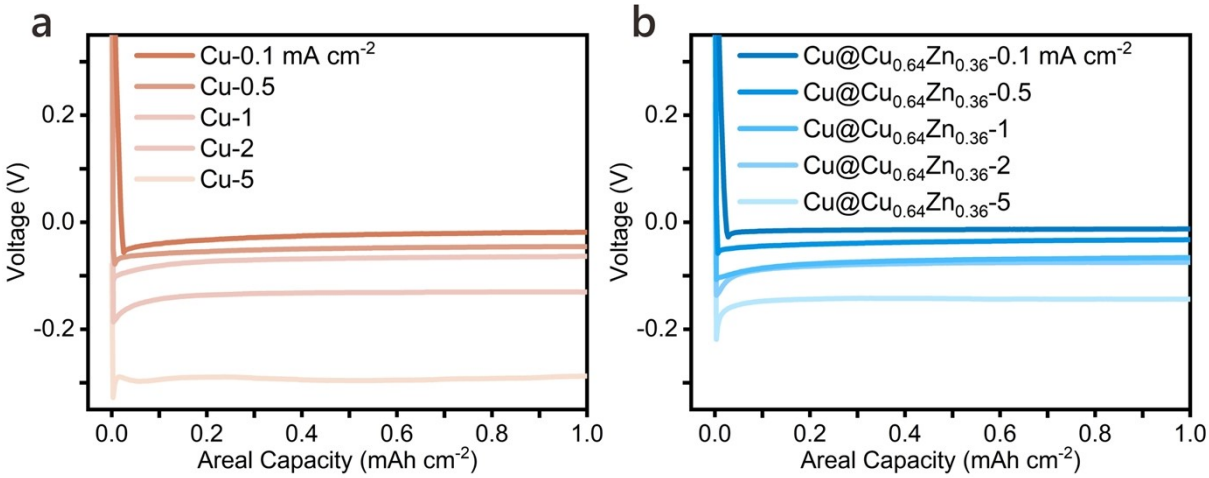

Fig. S21 Voltage-capacity profiles of Li||Cu cells using (a) Cu and (b) Cu@$Cu_{0.64}Zn_{0.36}$ at varying current densities.

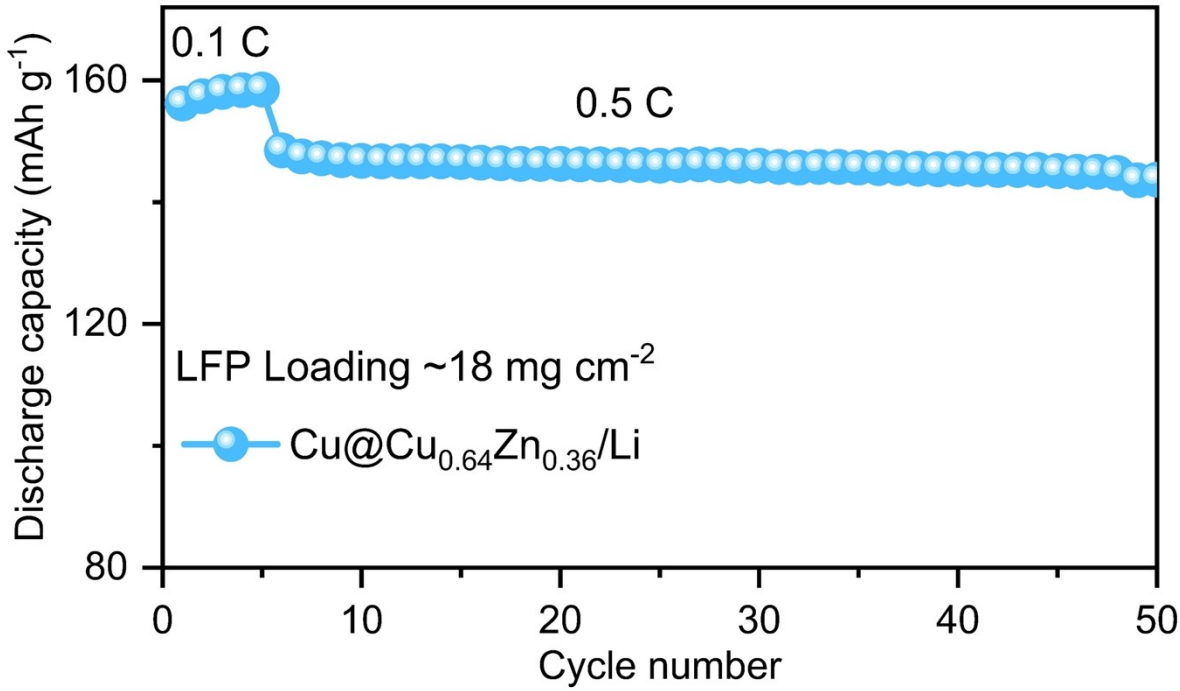

Fig. S22 Cycling stability of the Li||LFP full cell at 0.5 C with an LFP mass loading of ~18 mg cm^{-2} and a Li anode formed by pre-depositing 4 mAh cm^{-2} Li onto $Cu@Cu_{0.64}Zn_{0.36}$.

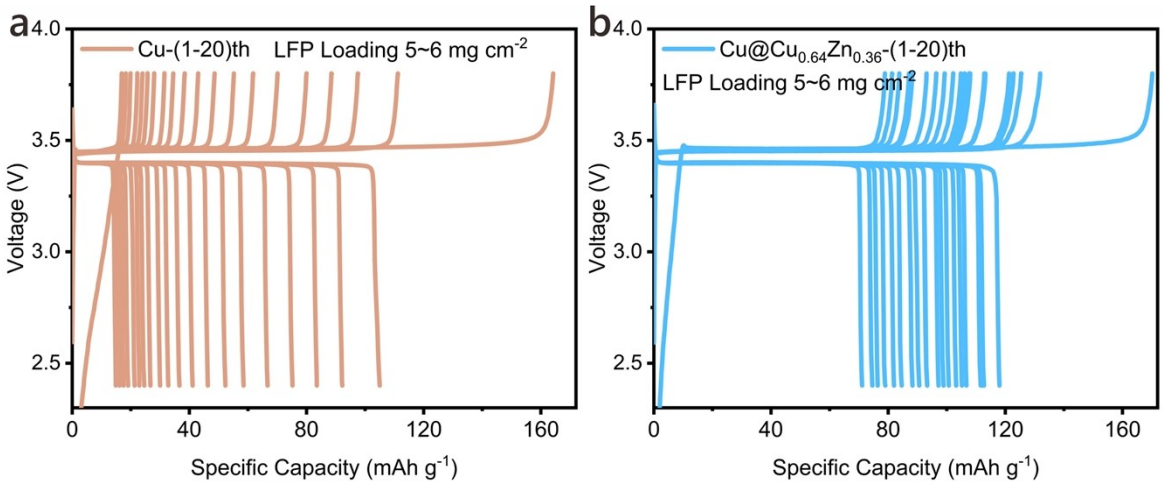

Fig. S23 Electrochemical performance of anode-free Li metal batteries with (a) Cu, and (b) $Cu@Cu_{0.64}Zn_{0.36}$ current collectors.

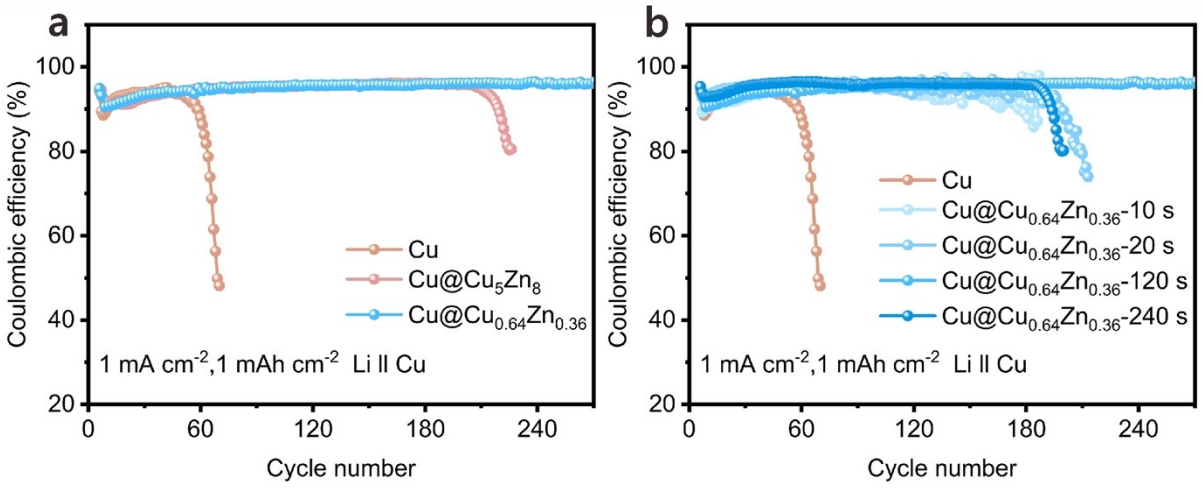

Fig. S24 (a) CEs over long cycles of different types of CCs at 1 mA cm^{-2}, 1 mAh cm^{-2}. (b) CEs over extended cycling for $Cu@Cu_{0.64}Zn_{0.36}$ obtained at different times during the first step of Joule heating on Cu foil (10 s, 20 s, 120 s, 240 s) in Li||Cu cells at 1 mA cm^{-2}, 1 mAh cm^{-2}.

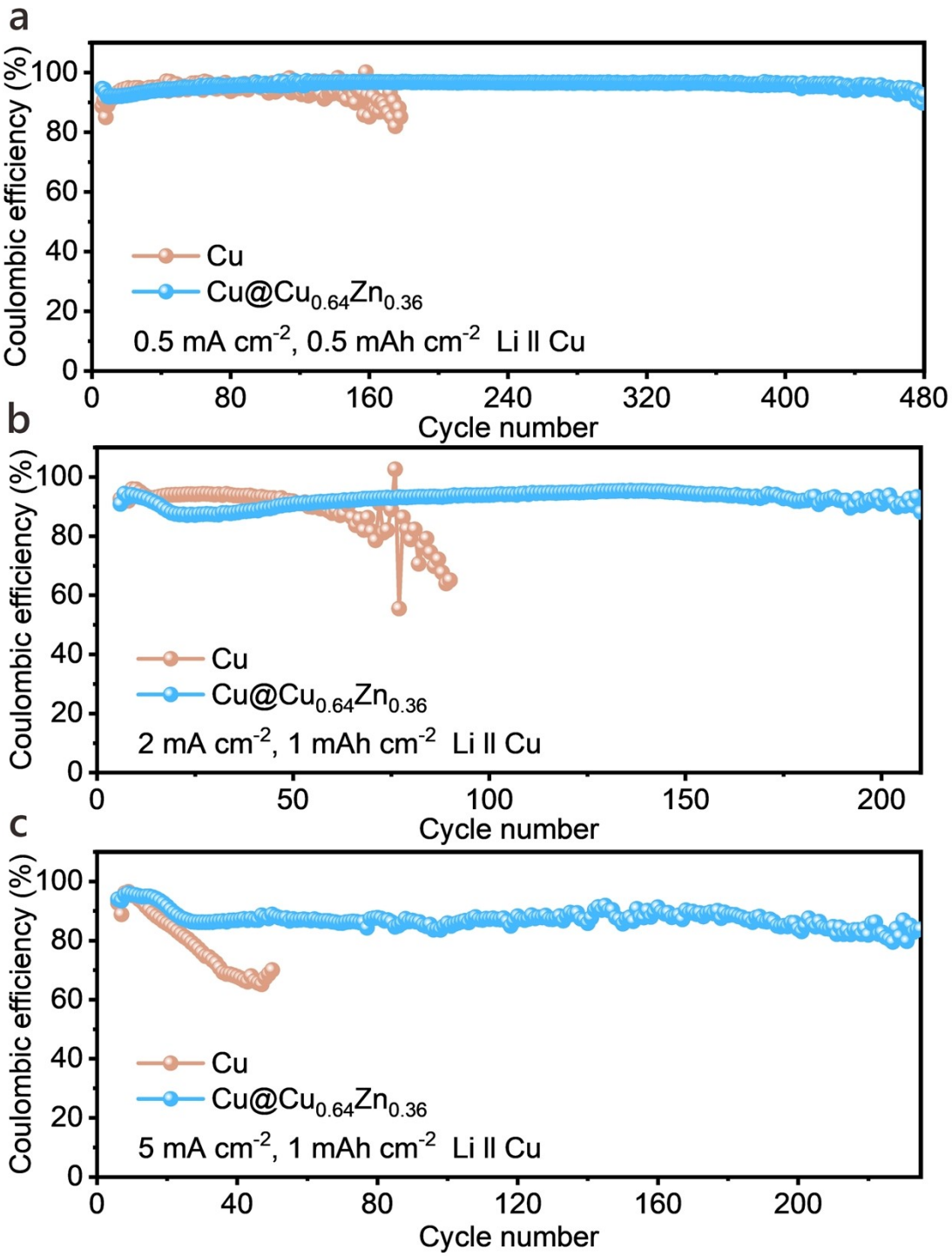

Fig. S25 Comparison of the cycling stability and CE of various Li||Cu cells using different Cu CCs at current densities of (a) 0.5, (b) 2 and (c) 5 mA cm^{-2}, with a fixed cycling capacity of 1 mAh cm^{-2}.

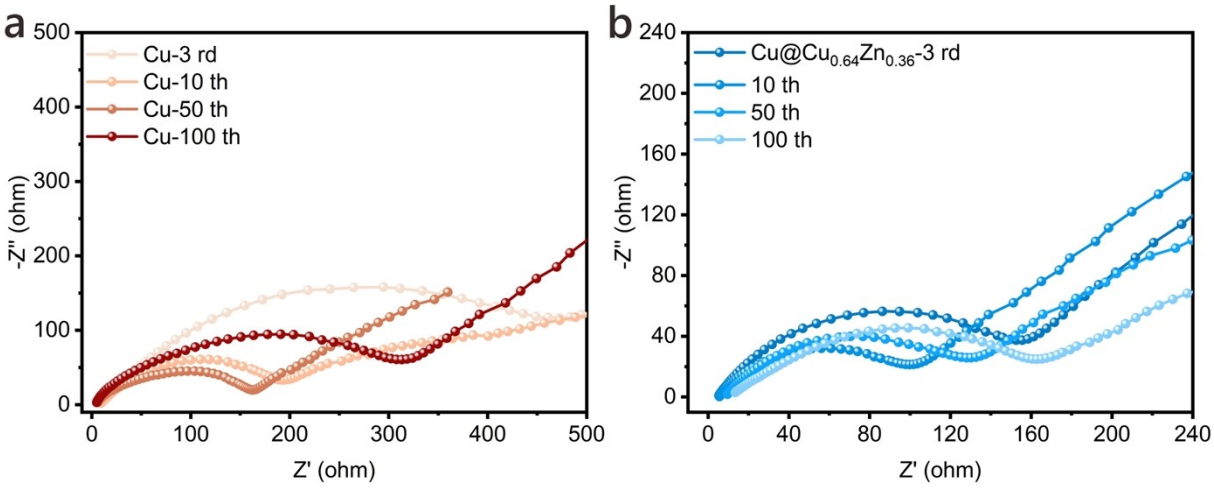

Fig. S26 Nyquist plots for the EIS response of Li||Cu cells with (a) Cu and (b) $Cu@Cu_{0.64}Zn_{0.36}$ after different cycles.

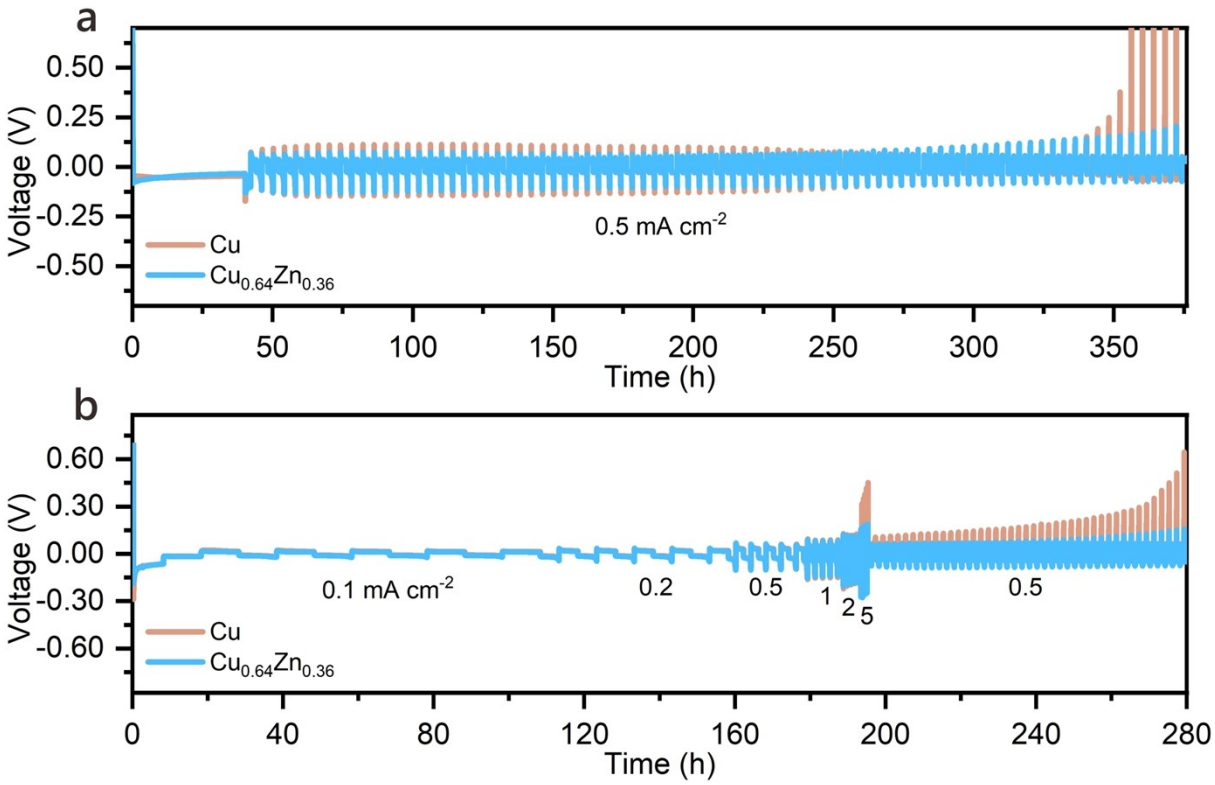

Fig. S27 (a) Cycling stability of thin film Li||Li symmetric cells with 4 mAh cm^{-2} Li pre-deposited of on Cu CCs at 0.5 mA cm^{-2}, 1 mA h cm^{-2}. (b) Rate capabilities of thin film Li||Li symmetric cells with 4 mAh cm^{-2} Li pre-deposited of on Cu CCs at varying current densities.

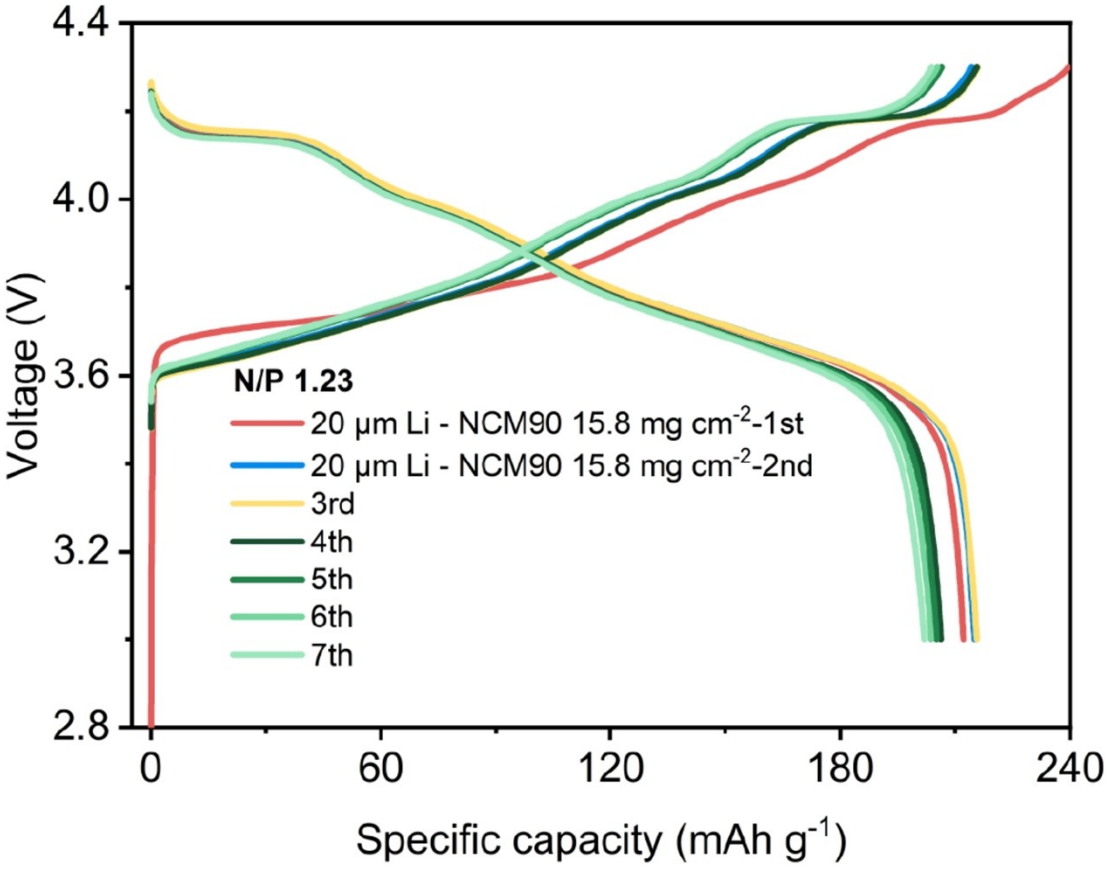

Fig. S28 The charge-discharge profiles of the Li||NCM90 pouch cell with the NCM90 mass loading of 15.8 mg cm^{-2} and Li anodes formed by pre-depositing 4 mAh cm^{-2} Li on Cu@$Cu_{0.64}Zn_{0.36}$.

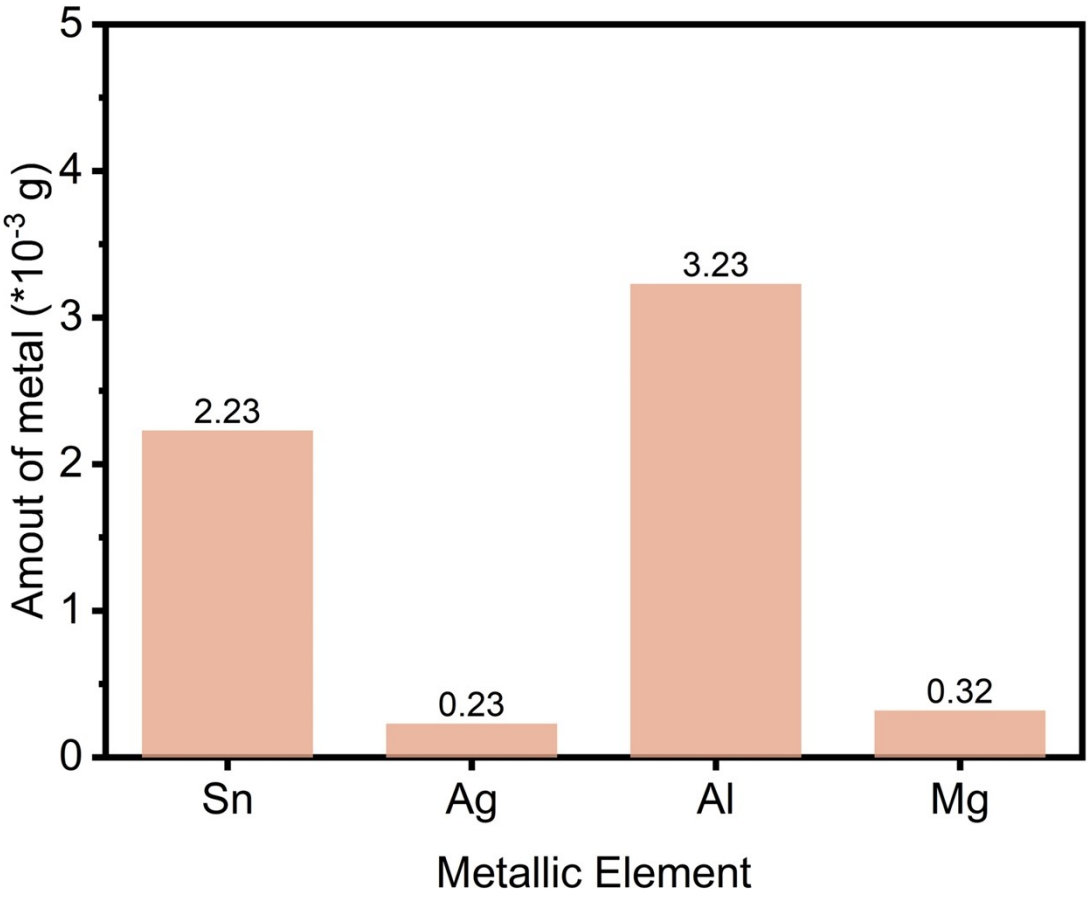

Fig. S29 ICP-OES results of the metal content in various Cu-based alloys.

References

1. M. Liu, J. F. Zhang, Z. Sun, L. Huang, T. Xie, X. W. Wang, D. Wang and Y. P. Wu, *Small,* 2023, **19**, 2206922.
2. X. Zhan, M. Li, X. Zhao, Y. Wang, S. Li, W. Wang, J. Lin, Z.-A. Nan, J. Yan, Z. Sun, H. Liu, F. Wang, J. Wan, J. Liu, Q. Zhang and L. Zhang, *Nat Commun.,* 2024, **15**, 1056.
3. B. D. Adams, J. Zheng, X. Ren, W. Xu and J. G. Zhang, *Adv. Energy Mater.,* 2017, **8**, 1702097.
4. G. Kresse and J. Hafner, *Phys Rev B Condens Matter* 1993, **47**, 558.
5. G. Kresse and J. Hafner, *Phys Rev B Condens Matter* 1994, **49**, 14251.
6. G. Kresse, *PhysRevB* 1996, **54**, 54.
7. P. E. Blochl, *Phys Rev B Condens Matter* 1994, **50**, 17953.
8. K. G and F. J, *Comput. Mater. Sci.,* 1996, **6**, 15.
9. K. B. John P. Perdew and Matthias Ernzerhof, *Phy. Rev. Lett.*, **77**, 3865.
10. S. Liu, X. Zhang, R. Li, L. Gao and J. Luo, *Energy Storage Mater.,* 2018, **14**, 143.